Colloids and Surfaces A: Physicochemical and Engineering Aspects 705 (2025) 135553

Contents lists available at ScienceDirect

Colloids and Surfaces A: Physicochemical and Engineering Aspects

journal homepage: www.elsevier.com/locate/colsurfa

Nanocomposite conductive r(GO/BSA) hydrogel as an effective dressing for rapid chronic diabetic wound healing

Shubham Garg [a,1], Shikha Tripathi [a,1], Somesh Agrawal [b], Vinod Tiwari [b], Avanish S. Parmar [a,*]

[a] Department of Physics, Indian Institute of Technology (Banaras Hindu University), Varanasi 221005, India
[b] Department of Pharmaceutical Engineering, Indian Institute of Technology (Banaras Hindu University), Varanasi 221005, India

GRAPHICAL ABSTRACT

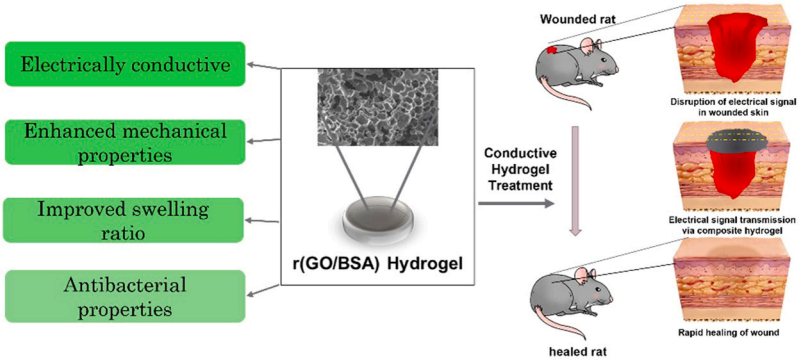

ARTICLE INFO

Keywords:
Conductive hydrogel
Protein self assembly
Diabetic wound healing
Anti-bacterial

ABSTRACT

Conductive hydrogels, with their soft, hydrated interface and superior electrical conductivity, represent a groundbreaking solution for diabetic wound healing. However, developing a conductive hydrogel with excellent biocompatibility has proven to be challenging. This study presents the synthesis of a novel conductive hydrogel composed of bovine serum albumin (BSA) protein and graphene oxide (GO) for the treatment of diabetic wounds. The prepared hydrogel is mildly reduced by ascorbic acid to facilitate charge-transfer and enhance its conductivity. Hydrogel is optimized for enhanced mechanical and electrical properties by changing the concentration of GO within the BSA matrix. The nanocomposite hydrogel demonstrates superior antibacterial properties and enhanced biocompatibility compared to the BSA hydrogel. The prepared hydrogel is investigated for wound healing capacity in a rat model, where it demonstrates rapid healing of chronic diabetic wound. The improved therapeutic outcomes are attributed to the hydrogel's ability to facilitate cellular activities through enhanced electrical conductivity by maintaining continuous electrical signal at the wound site. The presented findings suggest that nanocomposite protein-based conductive hydrogel not only hold great potential for advanced diabetic wound care and have potential for future innovation in tissue engineering, regenerative medicine and beyond.

* Corresponding author.
E-mail address: asparmar.phy@itbhu.ac.in (A.S. Parmar).
[1] Equal contribution

https://doi.org/10.1016/j.colsurfa.2024.135553
Received 13 August 2024; Received in revised form 24 September 2024; Accepted 11 October 2024
Available online 13 October 2024

1. Introduction

Diabetic wounds are a prevalent complication of Diabetes Mellitus, arising due to impaired healing process associated with this condition. Severe nerve damage and poor blood circulation contribute to the development of deep wounds and chronic ulcers, particularly on feet. Additionally, a compromised immune response and high blood sugar levels create an environment conducive to bacterial growth, leading to infection that further complicate wound management and healing [1–5] . Around 73 million people are suffering from diabetic wounds in India alone in 2021, expected to rise to 93 million by 2030, which illustrates the extent of severity and challenge it poses for healthcare sector[6,7] . Traditional clinical methods for treating diabetic wounds which includes anti-infection dressing, glycemic control, negative pressure suction, surgical debridement, and oxygen therapy are plagued with several drawbacks, such as lengthy and arduous procedures, use of hazardous/non-biodegradable materials, expensive clinical instrumentation, and slow wound healing[1,6,8,9]. While traditional dressings such as gauze, cotton wool, and bandages are effective in basic protection, they lack the ability to maintain optimal moisture balance. As wound healing process involves complex interplay of biological, chemical, electrical and physical signals, there is a need for development of multifunctional biomaterial with capability of delivering multiple signals to the wounded area[5,10,11]. Especially, electric conductivity plays a crucial role in enhanced wound healing. The normal skin cells tissues have conductivity in range of 10^{-6} to 10^{-3} Scm^{-1}, which is disrupted in case of a wound. An electroactive dressing material can provide a channel for transmission of endogenous electrical signals in wounded area, thereby accelerating the wound healing[12–14]. Conductive Hydrogels have been one such dressing material which have gained attention for potential wound care application. Properties such as high-water content, good swelling ratio, biocompatibility, and tunable mechanical and electrical properties are desirable and can be provided by properly engineered hydrogels[12–15]. However, making a conductive hydrogel with excellent biocompatibility has been a major challenge [16,17].

Here, we propose fabrication of a nanocomposite conductive protein-based hydrogel. BSA (Bovine Serum Albumin), a globular protein that undergoes gelation to form hydrogel under certain condition, such as changes in temperature and pH has recently been attracting significant attention for its potential wound healing applications. Good mechanical strength, high swelling ratio and excellent biocompatibility make it a promising candidate for biomedical applications such as drug delivery, wound healing, and tissue engineering [18–20]. Owing to these properties, BSA hydrogel has been investigated for application as diabetic wound dressing in a recent study [21]. However, BSA hydrogel in itself is not conducive to electric current. Several nanomaterials have been incorporated in hydrogels to enhance their conductivity including, metal ions, metal oxides, carbon nanotubes, graphene derivatives and conductive polymers [16,17,22]. Especially, graphene derivatives are leading candidate for this purpose owing to their high electrical conductivity, chemical stability, and large surface area [23,24]. Graphene and its derivatives have been an essential component of biomaterials and are proven to be cyto-compatible[25,26]. Additionally, graphene derivates are recognized for improving the mechanical properties of the hydrogel and imparting them antibacterial properties[27–29]. Especially, Graphene oxide (GO), enriched with oxygen containing functional groups, is a versatile two-dimensional material with tunable chemical, electrical and mechanical properties. The oxygen groups present on the surface make them highly hydrophilic and soluble in water[27,29]. This hydrophilicity and solubility are essential for preparing solution-based hydrogels. Furthermore, the electrical properties of GO-incorporated hydrogels can be tuned by its mild reduction, making it conductive by partial restoration of its sp^2-bonded carbon atoms[30–32].

In this work, we report a novel approach for fabrication of protein-based conductive hydrogel. The composite hydrogel is prepared by incorporating graphene oxide into the BSA hydrogel, followed by its mild reduction. To this end, the following subsections discuss the effect of GO concentration on the mechanical, morphological, and electrical properties of composite hydrogel by extensive characterization. After optimization, the efficacy of composite hydrogel against gram-positive and gram-negative bacteria is examined. The biocompatibility of the prepared hydrogel is tested by performing in-vitro cell culture study. Finally, the composite hydrogel is used as a diabetic wound dressing and its effect on wound healing process are examined on a rat model. The prepared composite hydrogel shows great potential for diabetic wound healing, representing a major advancement in this critical medical field.

2. Experimental section

2.1. Materials

Bovine Serum Albumin (BSA), graphite, sulfuric acid (H_2SO_4, 98 %), sodium nitrate ($NaNO_3$), potassium permanganate ($KMnO_4$), hydrochloric acid (HCl, 30 %), Hydrogen peroxide (H_2O_2, 30 %), and L-ascorbic acid were purchased from Sigma-Aldrich. Streptozotocin (STZ) and citrate buffer were purchased from Sigma-Aldrich. Dimethyl sulfoxide anhydrous (DMSO) and Fetal Bovine Serum (FBS) were procured from SRL. LB broth and nutrient agar media were purchased from HiMedia laboratories. NIH-3T3 cell line was procured from NCCS Pune. Deionized (DI) water (> 18MΩ) was used to prepare all aqueous solutions. All the reagents were used as such without further purification.

2.2. Synthesis of graphene oxide

Graphene oxide was prepared by modified hummer's method, using graphite as precursor[33]. Briefly, in a three-neck flask, 1 g of graphite was mixed with 150 mL of H_2SO_4 (conc.) and 1.5 g of $NaNO_3$ for 15 min under constant magnetic stirring while maintaining temperature under 5 °C. Following this, 6 g of $KMnO_4$ was very slowly added to the mixture over a period of 30 min under continuous stirring until the mixture turned into a dark green paste. The prepared mixture was diluted with 180 mL of DI water, accompanied by dropwise addition of H_2O_2. The resulting dark brown mixture was filtered and washed with HCl and DI water until the neutral pH was achieved. The mixture was further sonicated and centrifuged to remove excess $KMnO_4$ and metal ions. The sediment was air-dried overnight to obtain graphite oxide. Finally, the obtained powder was dispersed in DI water and sonicated in a water bath to obtain graphene oxide dispersion.

2.3. Synthesis of r(GO/BSA) hydrogel

Lyophilized BSA powder was dissolved in DI water at 300 mg/mL concentration. A stock solution of 10 mg/mL Graphene oxide was prepared in DI water. Next, an assortment of samples of 200 mg/mL BSA was prepared in petri dishes with varying concentrations of GO (namely 0.1, 0.5, and 1 % (w/v)). The petri dishes were incubated in a hot air oven preheated at 80 °C for 30 min. After incubation, the obtained GO/BSA hydrogels were placed in ambient condition to bring them to room temperature. A control hydrogel was also prepared, where instead of GO, equivalent amount of DI was added to maintain a constant concentration. Eventually, GO/BSA hydrogels were chemically reduced to r(GO/BSA) by incubation in a 2 $mgmL^{-1}$ ascorbic acid solution at 37 °C for 24 h. The hydrogels were washed several times by DI water and stored at 4 °C for further application. For further discussion, the hydrogels were named BSA for control, $(GO/BSA)_x$ and $r(GO/BSA)_x$ hydrogel respectively, where x represents the concentration of GO in the sample hydrogel.

2.4. Graphene oxide characterization

The optical absorbance of the prepared graphene oxide (GO) was recorded using an *Eppendorf biospectrometer* in the wavelength range of 200–800 nm. To obtain detailed crystallographic information, X-ray diffraction technique analysis was performed using a *Rigaku Miniflex 600* with a Cu-kα radiation source. Raman spectroscopy was conducted to analyze the structural defects of GO. DLS measurements were performed using *Malvern Panalytical Zetasizer pro* to examine the hydrodynamic size distribution and polydispersity index (PDI) of graphene oxide. The surface morphology of GO samples was examined using a scanning electron microscope (*NovananoSEM*), which provided detailed images of surface features. Furthermore, transmission electron microscopy (*Tecnai G2 20 TWIN*) was utilized to investigate the morphology at a higher resolution.

2.5. Hydrogel characterization

The porosity and cross-sectional surface morphology of the hydrogels were investigated using an *EVO MA15/18* scanning electron microscope. Pore distribution data were analyzed and tabulated using ImageJ software. The rheological properties of the prepared hydrogels were measured using a parallel plate geometry setup in an *Anton paar MCR 72 Rheometer***.** Initially, the linear viscoelastic range (LVR) was determined by applying a constant frequency of 10 rad/s. Subsequently, a frequency sweep was performed across a range of 0.1 rad/s to 10 rad/s at a constant strain in LVR to determine the storage and loss modulus, G' and G" respectively. Additionally, the shear thinning behavior was investigated in shear rate range of 0.1 – 100 s^{-1}.

The mechanical strength of prepared hydrogels was studied through compression tests performed on a texture analyzer (*Shimadzu, Japan*) with a maximum load capacity of 500 N. For these tests, the hydrogels were cut in cylindrical shape with a diameter of 10 mm and a height of 5 mm. The compression measurements were carried out at a constant speed of 1 mm/min. Additionally, cyclic compression tests were performed by subjecting hydrogels to 50 % deformation over three cycles.

The swelling ratio and water retention property of prepared hydrogels were investigated. For this purpose, the lyophilized samples were first soaked in DI water for 24 h to allow them to reach equilibrium swelling. Following this, the samples were carefully removed from the water and superficial water was removed by using kimwipes. The swollen samples were then weighed.

The swelling ratio, S was calculated using the formula,

$$S = \frac{w_t - w_0}{w_0}$$

Where, w_0 and w_t are the weight of dry and swollen hydrogel samples, respectively.

Water retaining ratio (WRR) was also calculated for all hydrogels. For this, swollen hydrogels were periodically weighed over a time period of 15 days at an interval of 2 days. Each measurement was conducted in triplicate for all hydrogel samples.

Conductivity measurements were performed using a digital multimeter (*FLUKE 287 true rms multimeter*). For this purpose, the hydrogel samples were cut in cuboid shapes with fixed length and cross-section area. Triplicate readings for resistance were measured at the end points of each sample and averaged. The conductivity, σ, was computed using the following relation:

$$\sigma = \frac{L}{R.A}$$

where R is the measured resistance, L and A are length and cross-sectional area of sample.

To measure the ionic conductivity of the prepared hydrogels, electrochemical impedance spectra were recorded by applying an alternate sinusoidal potential of 10 mV in the frequency range of 1–10^5 Hz using a computer-assisted MULTI AUTOLAB M204 (*Metrohm Autolab*) system. For this purpose, disc shaped samples of 10 mm diameter and 5 mm thickness were prepared, and placed between two parallel silver electrodes.

2.6. Antibacterial activity assay

The antibacterial efficacy of the r(GO/BSA) composite hydrogel were evaluated against Gram-positive (S. aureus) and Gram-negative (E. coli) bacteria using the agar disc diffusion method and kinetic growth inhibition studies. Overnight cultures of E. coli and S. aureus were grown in Luria-Bertani (LB) medium and incubated at 37 °C. These cultures were then diluted to an optical density (OD) of 0.6 (at 600 nm) and treated with various concentrations of the rGO-BSA hydrogel. As a positive control, ampicillin was used. The treated cultures were incubated at 37 °C, and the optical density was measured after 24 h using a microplate reader.

For the agar disc diffusion assay, 200 μL of each bacterial culture (OD 0.6) was evenly spread onto the agar plates. Whatman filter paper disks (6 mm in diameter) were soaked in 1 mg/mL hydrogel solutions and placed on the plates. Additionally, disc soaked in ampicillin solution served as positive control. The plates were incubated at 37 °C for 24 h. The inhibition zones around the disks were measured to determine antibacterial efficacy.

2.7. In vitro study

The biocompatibility of BSA, GO/BSA, and r(GO-BSA) hydrogel formulations was examined using the NIH-3T3 cell line and assessed via the MTT assay. NIH-3T3 embryonic mouse fibroblast cells were seeded in 96-well plates at a density of 1×10^4 cells per well in 100 μL of complete medium and incubated for 24 h. Post incubation, the cells were treated with three concentrations (5 μL/mL, 10 μL/mL, and 20 μL/mL) of each formulation for 24, 48, and 72 h to assess the time-dependent effects of the formulation on cell viability. Following treatment, the medium was replaced with 100 μL of MTT solution (0.5 $mgmL^{-1}$), and the cells were incubated for an additional 4 hours at 37 °C in a 5 % CO_2 atmosphere to allow the yellow MTT tetrazolium salt to be reduced by viable cells to purple formazan crystals. Following this, the MTT solution was carefully removed and 100 μL of DMSO:MeOH (1:1) solution was added to dissolve the formazan crystals. The absorbance of the resulting-colored solution was measured at 570 nm using a multiplate reader.

The cell viability was calculated by the following relation:

$$\%cell\ viability = \frac{A_S}{A_C} * 100$$

where A_S and A_C represents the absorbance of treated sample and control at 570 nm, respectively.

2.8. In vivo study

Rat model was used to conduct the in-vivo assessment of composite hydrogel. This project was approved by Institutional Animal Ethics Committee (IAEC), IIT (BHU) Varanasi (*IIT(BHU)/IAEC/2023/II/055*) for conducting wound healing tests on male SD rats. Rats were acclimatized under standard condition with free access to commercial pellet food and water. Type-II Diabetes was induced in rats using streptozotocin (STZ) injection at a 60 mg/kg body weight dose dissolved in a 0.1 M citrate buffer (pH 4.5). To confirm the successful induction of diabetes, blood glucose levels were monitored three days post STZ injection. Blood samples were obtained via tail vein sampling. Only those rats with fasting blood glucose levels above 250 mg/dL were considered diabetic and included in study. On the 8th day post-STZ injection, a full-

thickness excisional wound was created on the rats' back and disinfected with 70 % ethanol. Diabetic animals were divided into three groups: (1) negative control (no treatment), (2) BSA hydrogel-treated wounds, and (3) r(GO/BSA) composite hydrogel-treated rats. Treatments were applied topically every other day until the complete wound healing was observed. Throughout the experimental period, blood glucose levels and body weight were measured regularly to monitor the health status of rats. At the experiment's conclusion, rats were fasted overnight to stabilize the metabolic rate. Subsequently, the animals were sacrificed as per the guidelines of ethics committee and wound tissues were excised for histopathological analysis.

3. Result and discussion

The main objective of this work was to fabricate a conductive, protein-based hydrogel with biocompatibility, superior water retention, enhanced swelling properties and excellent mechanical strength. These properties were extensively investigated by employing various chemical, mechanical, and biological characterization techniques. The fabricated hydrogel was then evaluated for its potential application as a diabetic wound dressing. For achieving this purpose, we synthesized graphene oxide from graphite using modified hummer's method and the synthesized GO was incorporated into BSA hydrogel matrix. This composite hydrogel was subsequently reduced to form r(GO/BSA) hydrogel which is examined as a potential diabetic wound dressing. The following sections are therefore dedicated to the extensive characterization of synthesized graphene oxide and r(GO/BSA) hydrogel.

3.1. Graphene oxide characterization

Graphene oxide was exfoliated from graphite using modified hummer's method. The absorption spectra of the GO dispersion (in DI water) as presented in Fig. 1**a** exhibited a characteristic peak at 230 nm which is associated with π -π* transitions of the aromatic C = C bonds in the GO structure. A broad shoulder was also observed at 305 nm which is attributed to n- π* transitions of C = O bonds [34,35]. These features are distinct to the GO spectra indicating successful synthesis of graphene oxide. X-ray diffraction (XRD) spectra, as presented in Fig. 1b revealed a prominent sharp peak at 2θ = 10.63° which is attributed to the (001) plane of GO, indicating an interlayer spacing of 8.2 Å. The significant increase in d-spacing compared to pristine graphite (3.4 Å) is due to the incorporation of oxygen-containing functional groups such as hydroxyl, epoxy, and carboxyl groups. The spectra also showcased a smaller peak at 42.8°, which is attributed to the (100) plane of graphene oxide. The presence of a small peak at 2θ = 20.5° can be attributed to the (002) plane of graphite, indicating the presence of unoxidized graphitic particles alongside [36].

Raman spectroscopy is an important tool for characterizing the structural properties of graphene oxide. As presented in Fig. 1**c**, the Raman spectra of graphene oxide exhibited two bands. The D band centered at 1348 cm^{-1} is attributed to the defects and disorders present in the graphene lattice and is a characteristic feature of graphene oxide, whereas G band is associated with the in-plane stretching vibrations of sp^2 carbon atoms present in graphene lattice and it is found to be centered around 1580 cm^{-1} [37]. The high I_D/I_G ratio (~ 1.05) in this case indicated significant structural disorder created by incorporation of oxygen groups in the graphene lattice. The size distribution analysis of the graphene oxide dispersion in DI water as performed by dynamic light scattering is provided in Fig. 1**d**. The plot revealed a uniformity in the GO dispersion, with the hydrodynamic radius centered around 150 nm. Next, SEM image (Fig. 1**e**) of the prepared GO showcased two-dimensional morphology with wrinkled and curved texture. This morphological information was complimented by the TEM images which revealed layers of GO stacked onto one another with the typical wrinkled morphology (Fig. 1**f**). This extensive chemical and morphological analysis confirmed the successful synthesis of graphene oxide,

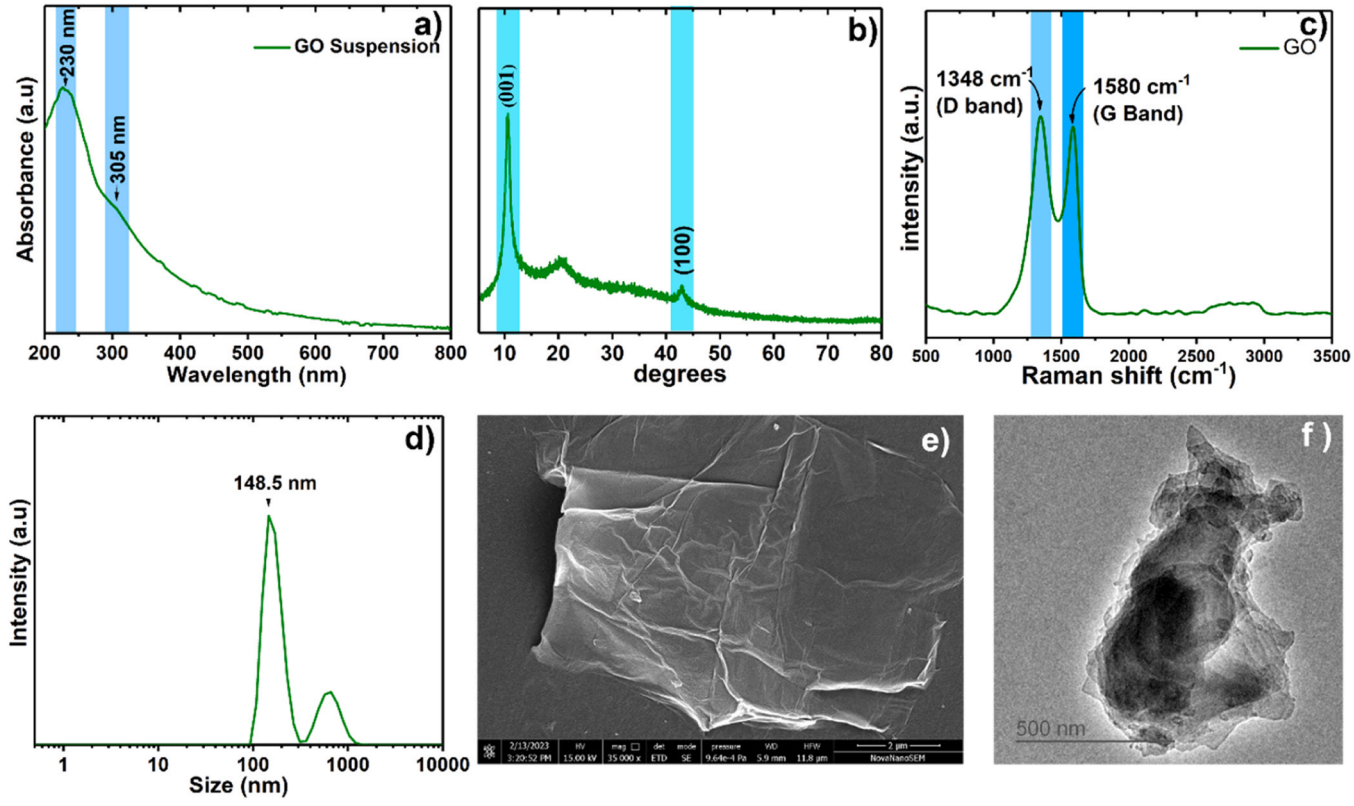

Fig. 1. a) UV/vis spectra, **b)** XRD spectra, and **c)** Raman spectra of synthesized graphene oxide; **d)** size distribution of GO suspension, **e)** SEM image and **f)** TEM image of GO.

which was further employed in the fabrication of composite hydrogel.

3.2. Hydrogel optimization and characterization

The morphological and mechanical properties of hydrogels play an integral role in the therapeutical effects of diabetic wound dressing. To optimize these properties, various tests were conducted to evaluate the effect of different concentrations of graphene oxide while maintaining a constant concentration of BSA. Four hydrogel samples were prepared with GO concentrations of 0, 0.1, 0.5, and 1.0 % (w/v) in 20 % (w/v) BSA solution (Fig. 2**a**). A mild reduction of the GO/BSA hydrogels was carried out by dipping the samples in 2 $mgml^{-1}$ ascorbic acid solution at 37 °C for 24 h. This treatment changed the color of hydrogel from light brown to black **(**Fig. 2**b)**, indicating that the reduction was successful. To understand the effect and extent of reduction, Raman spectra were recorded for $(GO/BSA)_{0.5}$ samples incubated in ascorbic acid solution for 0, 12, 24, and 36 h as presented in Fig. 2**c**. All recorded spectrum exhibit two distinct peaks corresponding to D and G band, centered around 1350 cm^{-1} and 1580 cm^{-1} respectively. The presence of the D band is attributed to defects and disorder in the otherwise pristine sp^2-bonded graphene structure, indicating the extent of oxidation. As the incubation period increased from 0 to 36 h, the intensity of D band decreased, suggesting a reduction of sp^3 bonds and partial restoration of graphene structure. A comparative analysis of I_D/I_G ratio (Fig. 2**d**) clearly suggests that the hydrogels incubated in ascorbic acid for longer durations exhibit reduced defects, indicating the successful reduction reaction.

3.2.1. Surface morphology and porosity

After the validation of reduction, the morphology of all hydrogels were investigated using scanning electron microscope. These are presented in Fig. 2**(e, f, g, h)**. The microscopic images of hydrogel's cross-sectional area exhibited interconnected porous structure. This 3D porous structure is typical of heat-induced gelation of BSA protein[21, 38]. As the concentration of graphene oxide in the matrix increased, the pore size of the hydrogel decreased significantly. The statistical analysis using imageJ software showcased decrement in pore size with increment in GO concentration **(**Fig. 2**(i, j, k, l))**. Evidently, the average pore size decreased from 75 μm in control hydrogel to 28 μm in $r(GO/BSA)_{1.0}$. This decrease in pore size can be attributed to the supramolecular interaction between graphene oxide sheets and BSA hydrogel, leading to stronger crosslinking density and thus reduced pore size. Notably, increase in the pore density is a desirable property suitable for enhanced water encapsulation. Moreover, the absence of any aggregates or chunks in the microscopic structure of rGO/BSA hydrogels suggested a uniform dispersion of rGO in the BSA matrix.

3.2.2. Rheological properties

A wound dressing applied on the wounded area is often subjected to variable tension as the body moves around. Therefore, an efficient wound dressing must have acceptable structural, mechanical and biological strength so that it can conform to such tensions. These properties were analyzed by performing rheological studies of the prepared hydrogels. First and foremost, to find the linear viscoelastic range (LVR), amplitude test was performed for all the samples at a constant frequency of 1 $rads^{-1}$. The amplitude was varied in range of 0.1–150 % shear strain (Fig. 3**a**). The storage modulus was found to be greater than the loss modulus in all cases, indicating the elastic nature of our hydrogel. Both the storage and loss modulus were constant till 35 % shear strain which depicts its LVR region. This is important for its application as a wound dressing. A certain increase in storage modulus and the shift of breaking point towards higher values of shear strain with increasing GO content

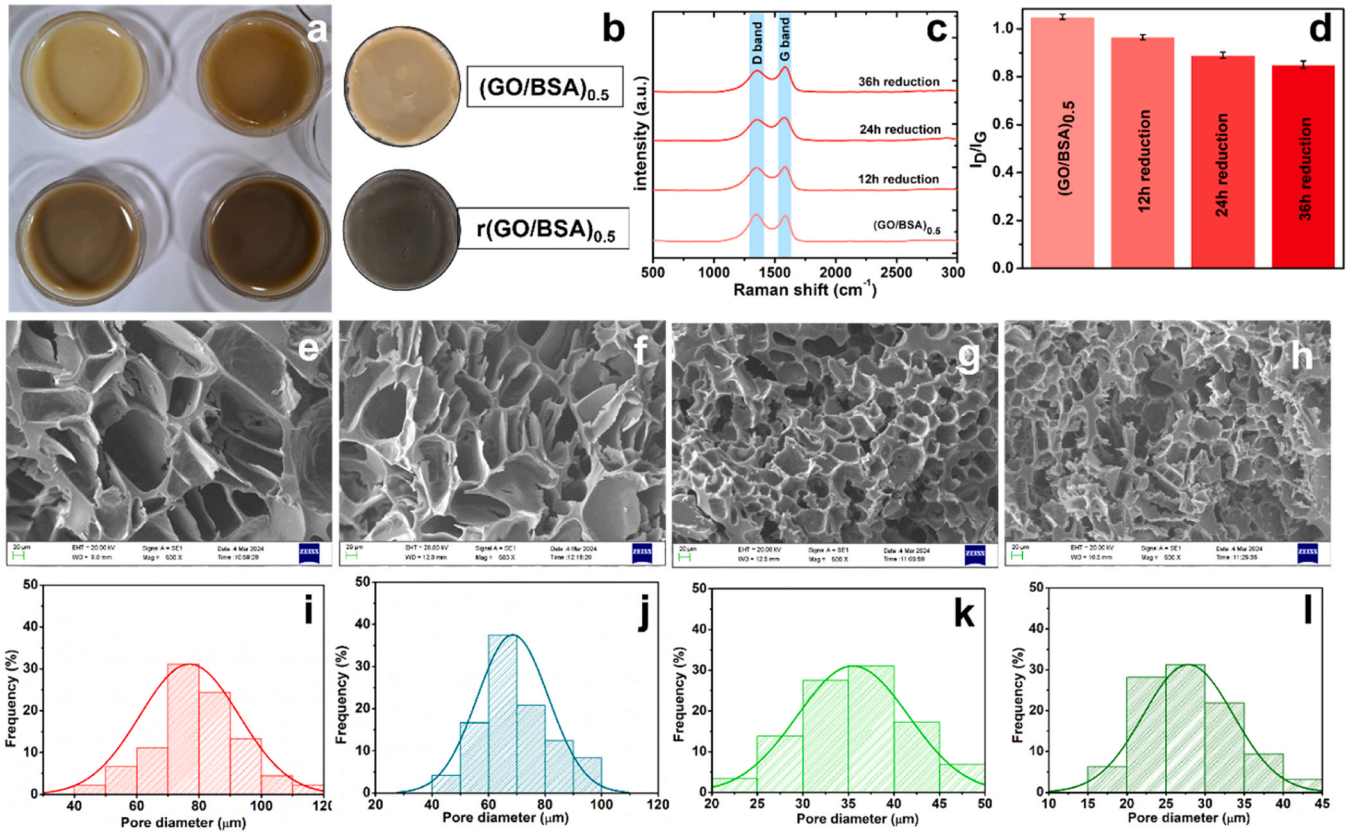

Fig. 2. a) Photographs of BSA protein hydrogels with varying concentration of GO (0, 0.1, 0.5, 1.0 % GO (w/v)) **b)** partial reduction of $(GO/BSA)_{0.5}$ hydrogel by ascorbic acid, **c)** raman spectra of $(GO/BSA)_{0.5}$ compared to its reduced forms, **d)** comparative plot of I_D/I_G ratio for different duration of reduction; SEM images of crosssectional area of hydrogels and their corresponding pore distribution **e),i)** BSA **f),j)** $r(GO/BSA)_{0.1}$ **g),k)** $r(GO/BSA)_{0.5}$ and **h),l)** $r(GO/BSA)_{1.0}$.

point towards enhanced crosslinking density of hydrogel due to incorporation of graphene oxide. Next, frequency sweep was carried out with amplitude kept fixed at 10 % (within LVR region). The storage and loss modulus were plotted against angular frequency (Fig. 3**b**). Here again, we witnessed an increase in the storage modulus with increasing GO content; control hydrogel showcasing a G' of 80 Pa, whereas r(GO/BSA)$_{1.0}$ having storage modulus of 150 Pa. G' remained dominant over G" across frequency range of 0.1–20 rad s^{-1} which indicated that the hydrogels were stable and behaved as viscoelastic solid. Furthermore, both G' and G" were nearly constant in the entire frequency range, thereby showcasing stability over long-term storage due to stable crosslinked network. In addition, hydrogel viscosity behavior with changing shear rate was also recorded (Fig. 3**c**). The constant negative slope of viscosity vs shear rate plot revealed the shear thinning nature of our hydrogel which is a crucial property for fabricating extrusion-based wound dressings. The increase in viscosity with increasing GO content again confirmed our hypothesis that GO was playing a pivotal role in enhancing the crosslinking density of BSA hydrogel.

3.2.3. Compression test

A wound dressing is required to have good compressive strength, so that it can conform to external pressure. For this reason, the mechanical strength of hydrogels was recorded by conducting the compression test. All the hydrogels were cut in cylindrical shape of height 4 mm. As depicted in Fig. 3**d,** compared to control hydrogel, the composite hydrogel showcased increased mechanical strength. The r(GO/BSA)$_{1.0}$ hydrogel could sustain ~ 5*10^3 MPa of compressive stress upon 50 % deformation compared to only ~ 10^3 MPa sustained by control hydrogel. This five-fold increase in compressive strength of composite hydrogel can be attributed to enhanced crosslinking density and supramolecular interaction between BSA and graphene oxide. Additionally, the cyclic compression test was performed to assess the shape memory of r(GO/BSA)$_{1.0}$ hydrogel. As witnessed in the Fig. 3**e,** after first cycle of compression, the composite hydrogel exhibited only 11 % decline in sustained force for 50 % deformation. Only 3 % decline was noticed in the subsequent cycle. It can be inferred from this observation that the prepared composite hydrogel possesses considerable shape memory. This test confirms the excellent mechanical strength of our hydrogel owing to the non-covalent interaction between BSA and graphene oxide.

3.2.4. Swelling ratio and water remaining ratio

The encapsulated water plays a crucial role in maintaining the optimum moisture levels at wound site, reducing the chances of infection

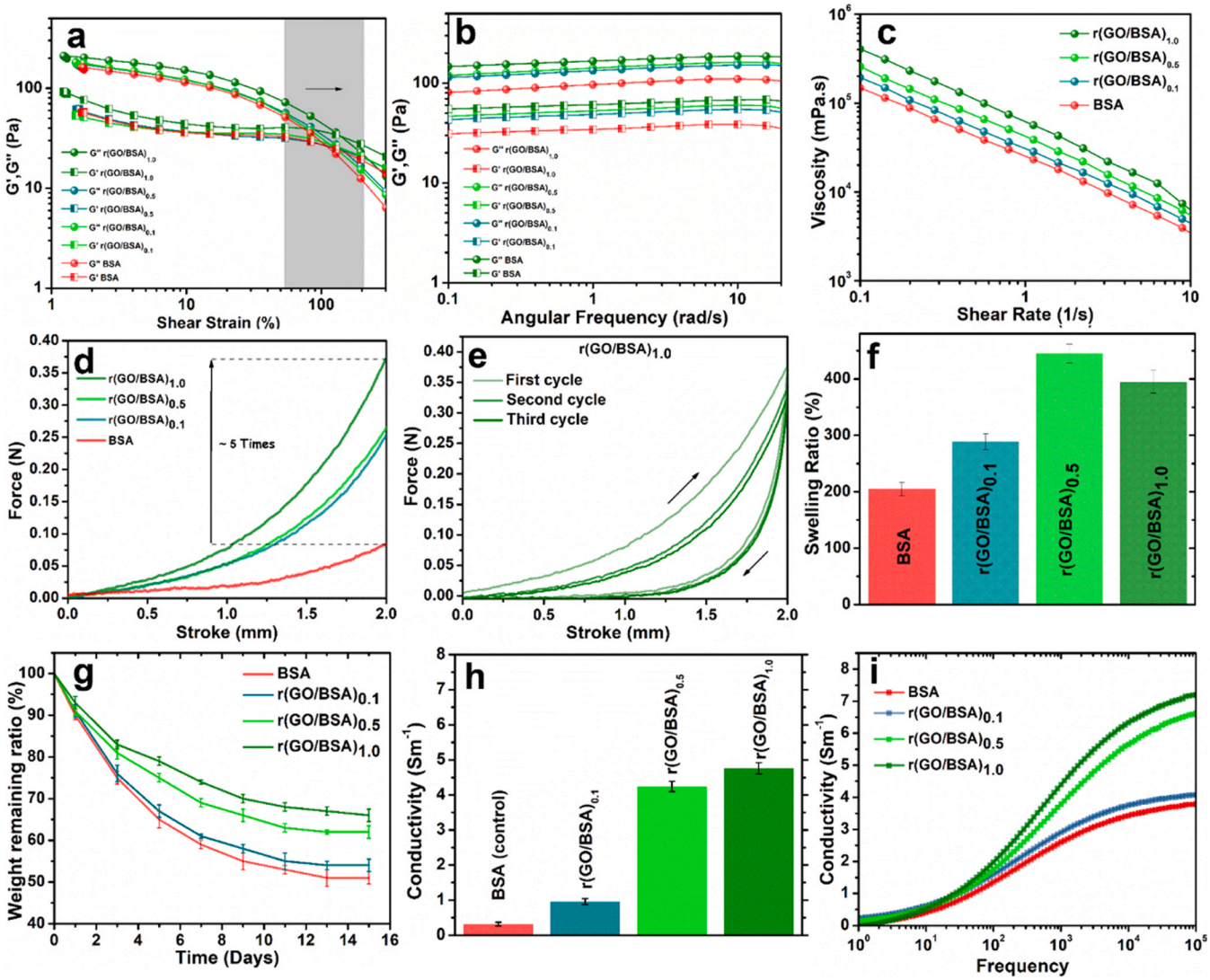

Fig. 3. The rheological properties of hydrogels comprised of various concentrations of GO, including amplitude sweep **(a),** frequency sweep **(b),** and viscosity versus shear rate plot **(c);** The compressive test for hydrogels showcasing relation between stroke and force **(d)**, and cyclic compressive test for r(GO/BSA)$_{1.0}$ hydrogel **(e);** swelling ratio **(f)** and water remaining ratio of hydrogels **(g)**; two probe conductivity measurement **(h)** and EIS measurement of conductivity **(i)** for all hydrogels.

and thereby escalating the wound healing process. To quantify this aspect, swelling ratio of the hydrogels was calculated. As presented in Fig. 3**f**, The swelling ratio of BSA hydrogel showcased significant enhancement with incorporation of graphene oxide. Evidently, the BSA hydrogel showcased a swelling ratio of 200 % which is owed to its three-dimensional crosslinked structure. r(GO/BSA)$_{0.1}$ and r(GO/BSA)$_{0.5}$ demonstrated an increased swelling ratio of 300 % and 400 %, respectively. This enhanced water encapsulation is attributable to the highly hydrophilic nature of GO owing to the oxygen rich surface functionalities. However, further increase in GO content as witnessed in case of r(GO/BSA)$_{1.0}$ witnessed a slight decrease in swelling ratio. It can be inferred from this observation that the pore size plays critical role in water holding capacity of hydrogel, and decrease in pore size beyond a certain point can lead to reduced swelling. Next, water remaining ratio of a hydrogel was assessed as it provides crucial information regarding proposed wound dressing. Rapid water loss can lead to premature degradation of the hydrogel which can impede the healing process. As demonstrated in Fig. 3**g**, the incorporation of GO significantly enhances the water retention properties of the hydrogel. With increasing concentrations of GO, the hydrogels exhibit an improved capacity to retain water over extended periods.

3.2.5. Conductivity test

As reported by various groups [13,31], conductivity can play a significant role in wound healing process. Our skin has its own conductive pathways for conveying bioelectrical signals across cell. At the wound site, these pathways get disrupted impeding the signal transmission, which can probably impede or delay wound healing process. Conductive hydrogels can help in forming these pathways which can potentially escalate the healing process. We tuned the electrical and ionic conductivity of our composite hydrogels by varying the amount of graphene oxide incorporated inside hydrogel matrix. The electric conductivity was measured by using digital multimeter using the relation,

$$\sigma = \frac{L}{R * a}$$

where, L, R, and a are the length, resistance and cross-sectional area of the hydrogel sample. As shown in Fig. 3**h**, the control hydrogel showcased high resistance. Compared to control hydrogel, r(GO/BSA) hydrogels demonstrated significant increase in conductivity with increasing concentration of GO within the hydrogel. This observed increase in conductivity can be attributed to several factors, the primary factor being the partial reduction of surface GO which restored some of the conjugated π-electron systems of graphene. Furthermore, graphene oxide can create strong interfacial interactions with the protein matrix, potentially facilitating better charge transfer. Next, the ionic conductivity of the hydrogels was measured by applying an AC signal **(**Fig. 3**i).** As depicted in the figure, the conductivity increased with increasing frequency for all samples. The increase in graphene oxide content significantly enhanced the ionic conductivity of hydrogel. While r(GO/BSA)$_{0.1}$ sample demonstrated little improvement compared to the control hydrogel, further increase in GO concentration resulted in substantially enhanced conductivity values. Specifically, the conductivity for BSA hydrogel was measured to be 2.7 Sm^{-1}, which increased to 4.7 Sm^{-1} for r(GO/BSA)$_{1.0}$, both measured at 1 MHz frequency. This significant enhancement in conductivity may be attributed to two reasons; first, reduced graphene oxide at the surface facilitates better charge transfer at the interface and second, graphene oxide is highly hydrophilic which can lead to improved water encapsulation, which in turn enhances the ionic conductivity of composite hydrogels.

We conducted extensive characterization of the prepared hydrogel samples for understanding the effect of GO in BSA hydrogel. All the hydrogels exhibited similar rheological properties, and were characterized as viscoelastic materials. The viscosity of the hydrogels increased with higher GO concentrations. Compressive test results indicate that the incorporation of graphene oxide into the BSA matrix does impart greater mechanical strength to the hydrogels. It also influenced the morphology of the BSA hydrogel by making the pores more uniform and compact, thus increasing the swelling ratio. However, it was noted that swelling ratio reached a saturation after 0.5 % GO (w/v) and decreased beyond this concentration. The conductivity of the composite hydrogel increased with increasing GO concentration.

These results favor the composite hydrogel over BSA hydrogel in terms of morphological, mechanical, and electrical properties. For wound dressing application, water retention is crucial for maintaining optimum moisture at the wound site, adsorbing wound exudates, and providing ionic conductivity. Also, it was witnessed that the conductivity of r(GO/BSA)$_{0.5}$ and r(GO/BSA)$_{1.0}$ are comparable. Therefore, for further biological studies, the r(GO/BSA)$_{0.5}$ hydrogel, which showcased greatest water swelling was selected. All subsequent tests and studies were performed using the r(GO/BSA)$_{0.5}$ hydrogel. Thus, to avoid the confusion, the subscript indicating GO concentration is dropped from here on and r(GO/BSA) is used for hydrogel containing 0.5 % GO, unless mentioned otherwise.

3.3. Antibacterial assay

We evaluated the antibacterial efficacy of BSA hydrogel, GO/BSA hydrogel, and r(GO/BSA) hydrogel, and compared it to the antibiotic ampicillin formulation against both gram-positive (Staphylococcus aureus) and gram-negative (Escherichia coli) bacteria. The bacterial growth in solutions having BSA, GO/BSA and r(GO/BSA) formulations was examined by measuring the optical density at 600 nm and compared to control solution (Fig. 4b). It was witnessed that the BSA hydrogel has negligible effect on bacterial growth, and its solution showcased OD similar to the control group. Bacterial solution exposed to r(GO/BSA) hydrogel exhibited significantly lower OD value compared to GO/BSA hydrogel. The agar disc diffusion method (Fig. 4a) was used to measure the inhibition zones for different samples. BSA hydrogel (i) did not show any inhibitory behavior against either of the bacteria strain, which confirmed its lack of antibacterial properties. Sample (iii) showed its characteristic inhibition rings of ampicillin antibiotic. Against E. coli, the measured inhibition zones for ampicillin, GO/BSA, and r(GO/BSA) were 29.36 mm, 18 mm and 27.52 mm, respectively. Against S. aureus, the they were measured to be 32.13 mm, 25.6 mm, and 31.95 mm respectively. It was noted that in both the bacteria case, r(GO/BSA) performed considerably well in inhibiting bacteria growth compared to (GO/BSA) hydrogel. Moreover, it demonstrated comparable efficacy to the antibiotic ampicillin. The results from the OD test and agar disc diffusion indicate that the incorporation of GO into BSA hydrogel significantly enhances its antibacterial properties. This is owed to the strong anti-bacterial properties of graphene oxide. Also, the partial reduction of GO on the hydrogel surface further elevated the antibacterial efficacy of composite hydrogel. These enhanced antibacterial properties are anticipated to play significant role in combatting the issue of bacterial infection in the wound site, which can impair the wound healing process [39]. These results suggest that the prepared composite hydrogel can also serve as effective antibacterial agent in the hydrogel, which can potentially boost the wound healing process

3.4. Invitro studies

The biocompatibility of biomedical materials is paramount for their successful application in medical treatments. The MTT colorimetric assay was employed to estimate the effect of hydrogels (specifically, BSA hydrogel, (GO/BSA) hydrogel and r(GO/BSA) hydrogel) on the viability of NIH-3T3 fibroblast cells. Cell viability was measured at multiple time points, with a focus on 72-hour mark for assessing any long-term effects of hydrogel on cell health (Fig. 4**c**). A time-dependent decrease in cell viability was observed across all hydrogel formulations. There was an initial increase in cell viability, suggesting a favorable interaction

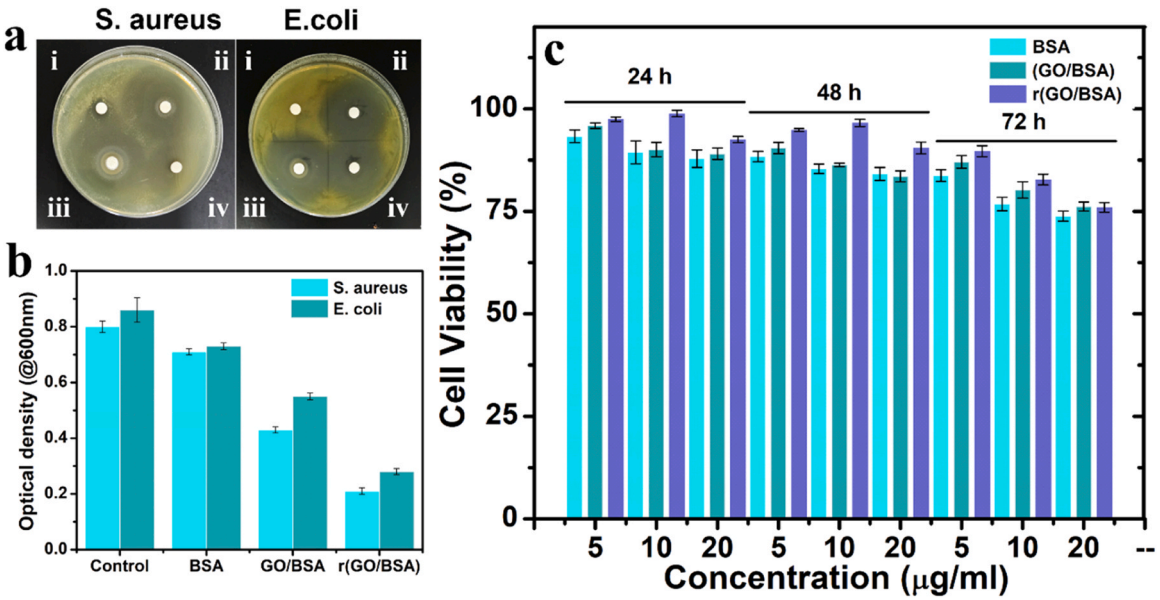

Fig. 4. Antibacterial properties and invitro cell viability test for different hydrogels, **a)** image showcasing effect of BSA hydrogel (i), r(GO/BSA) hydrogel (ii), ampicillin (iii), and GO/BSA hydrogel (iv) on gram-positive (S. aureus) and gram-negative (E. coli) bacteria inoculated in agar plates; **b)** the optical density recorded for S. aureus and E. coli bacteria solutions exposed to BSA, GO/BSA and r(GO/BSA) hydrogels respectively compared with control group; **c)** Cell viability of NIH 3T3 fibroblast cells exposed to various dose concentrations of BSA hydrogel, GO/BSA hydrogel, and r(GO/BSA) hydrogel.

between hydrogel and cells. However, at higher doses, cell viability decreased. After 72 h, a reduction in cell viability by approximately 20–25 % was noted. Despite this decrement, all hydrogel formulations maintained relatively high cell viability rates (74–77 %) even at the highest concentration. The observed cell viability test indicates a dose-dependent response to hydrogels. Nonetheless, the cell viability levels remained above 70 % which is indicative of low toxicity and acceptable biocompatibility. The high cell viability also suggests that hydrogels do not significantly impair fibroblast mitochondrial function and can be potentially used in biomedical applications.

3.5. *In vivo wound healing studies*

To evaluate the efficacy of prepared composite hydrogel, dressing of

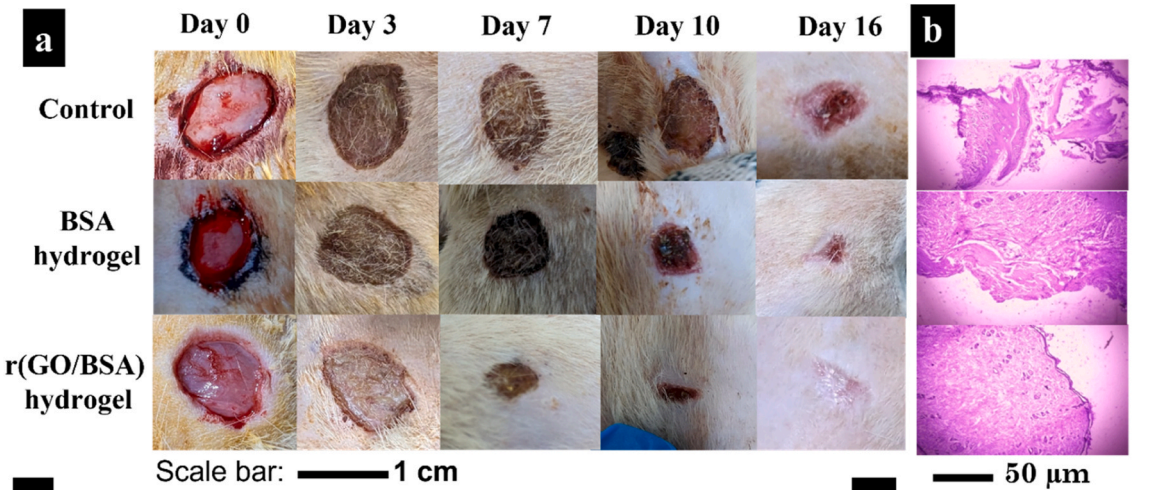

c

Group name	Weight (gm)	Blood glucose level (mg/dl)		
		Day 0 (before injection)	Day 7 (1 week after STZ injection)	Day 16 (before sacrifice)
Group 1	236±18	79.7±7.4	395±15.2	219±25.7
Group 2	251±30	73.8±7.9	411±23.6	303±27.4
Group 3	239±27	74.6±9.1	296±32.8	212±24.4

Fig. 5. The effect of different treatments on wound healing process of three groups of rats. **a)** Macroscopic images taken on day 0, 3, 7, 10, and 16 respectively (columns) showcasing the wound closing process for different formulations (rows). The control group is not given any treatment (scale bar: 1 cm). **b)** histopathological anatomy of wound tissue after the wound healing (scale bar: 50 μm). **c)** table consisting weight and blood glucose levels information for rats of three groups. **d)** the wound closure speed for three different groups.

BSA hydrogel, and r(GO/BSA) hydrogel were applied to diabetic wound in rats. A negative control (no treatment) was also evaluated for comparison. The wound areas were measured at 0, 3, 7, 10, 16 days after wound creation. Fig. 5**a** summarizes the residual wound area for three groups and its change with time. For the negative control (with no treatment), the wound closed gradually albeit very slowly. There was significant wound size on day 16. In the experimental groups, all groups showed good healing speed. Compared to BSA hydrogel, the wound closed much faster when treated with composite hydrogel. On day 10, the wound in composite hydrogel group were almost healed, whereas the group with BSA hydrogel treatment showed considerable wound size.

By day 16, wounds were completely sealed off in composite hydrogel treated group. Fig. 5**d** revealed the speed of wound closure in all three groups. It can be noted that r(GO/BSA) hydrogel showed escalated wound healing compared to the control groups. Histological analysis (Fig. 5**b**) revealed a fully integrated new epidermis in the hydrogel-treated groups, with the r(GO/BSA) hydrogel-treated group showing advanced healing and thicker granulation tissue.

From the above wound closure results, it can be noted that the BSA based hydrogel showed positive efficacy towards diabetic wound healing. This result is in agreement with the previous report [21]. This is attributed to its highly porous structure and high swelling ratio. From our results, it was also noted that the incorporation of graphene oxide in BSA hydrogel matrix and its partial reduction did help in escalating the re-epithelialization process, which resulted in considerably faster wound healing in r(GO/BSA) hydrogel-treated group. It is proposed that this faster healing response by composite hydrogel can be attributed to the conductive nature of our hydrogel which helps in transmitting endogenic bioelectrical signals to the wound. These bioelectrical signals are responsible for the movement of important cells such as keratinocytes, immune cells to the wound site which are involved in tissue repair. Continuous electrical signals are also known to promote cell proliferation and differentiation, crucial for tissue repair. Moreover, the electrical signals are responsible for release of protein and growth factors from cells which are key to healing process [40–42]. This study suggests that protein-based conductive hydrogels can be used as potential dressing material for treating diabetic wounds.

4. Conclusion

In this work, we prepared nanocomposite r(GO/BSA) conductive hydrogel dressings for treating diabetic wounds. The prepared composite hydrogel was extensively characterized for its morphological, mechanical and electrical properties. The composite hydrogel exhibited excellent mechanical strength, electrical conductivity and antibacterial properties. The conductive nature of composite hydrogel facilitates enhanced electrical simulation, which has been reported to accelerate the healing process in wounds. The hydrogel treatment accelerated the re-epithelialization process by facilitating endogenic biochemical signals in wound. To the best of our knowledge, this is the first report on synthesizing a composite protein-based conductive hydrogel with excellent biocompatibility and biodegradability. Its multifunctional properties emphasize the potential for developing next-generation biomaterials that can significantly improve patient outcomes and quality of life. This composite hydrogel not only opens new avenues for the diabetic wound healing, but also paves the way for future advancements in tissue engineering, regenerative medicine and more.

Ethical statement

We declare that this project was approved by Institutional Animal Ethics Committee, IIT (BHU) Varanasi (*IIT(BHU)/IAEC/2023/II/055*) for conducting wound healing tests on male SD rats. The CPCSEA guideline was strictly followed while handling the animals.

CRediT authorship contribution statement

Somesh Agrawal: Methodology, Formal analysis. **Vinod Tiwari:** Validation, Resources, Investigation. **Shubham Garg:** Writing – original draft, Investigation, Formal analysis, Data curation, Conceptualization. **Shikha Tripathi:** Validation, Investigation, Formal analysis, Data curation. **Avanish Parmar:** Writing – review & editing, Supervision, Resources, Project administration, Funding acquisition, Conceptualization.

Declaration of Competing Interest

The authors declare that they have no known competing financial interests or personal relationships that could have appeared to influence the work reported in this paper.

Acknowledgment

SG is thankful to UGC for the senior research fellowship**.** ST is thankful to PMRF fellowship. ASP is thankful to DST-SERB For TAR/2023/000015 grant for carrying out this project.

Note: The authors declare no competing financial interest.

Data availability

Data will be made available on request.

References

[1] C.C.L.M. Naves, The Diabetic Foot: A Historical Overview and Gaps in Current Treatment, Adv. Wound Care (N. Rochelle) 5 (2016) 191–197, https://doi.org/10.1089/wound.2013.0518.
[2] W.S. Joseph, B.A. Lipsky, Medical therapy of diabetic foot infections, J. Vasc. Surg. 52 (2010) 67S–71S, https://doi.org/10.1016/j.jvs.2010.06.010.
[3] C.K. Bowering, Diabetic foot ulcers -: Pathophysiology, assessment, and therapy, Can. Family Physician 47 (2001) 1007–1016.
[4] J.L. Burgess, W.A. Wyant, B.A. Abujamra, R.S. Kirsner, I. Jozic, Diabetic wound-healing science, Medicina 57 (2021), https://doi.org/10.3390/medicina57101072.
[5] D.K. Chellappan, Y. Yenese, C.C. Wei, G. Gupta, Nanotechnology and diabetic wound healing: a review, Endocr. Metab. Immune disord.-drug targets 17 (2017) 87–95, https://doi.org/10.2174/1871530317666170421121202.
[6] S. Basu, N. Sharma, Diabetes self-care in primary health facilities in India - challenges and the way forward, World J. Diabetes 10 (2019) 341–349, https://doi.org/10.4239/wjd.v10.i6.341.
[7] R. Vaishya, A. Misra, A. Vaish, S.K. Singh, Diabetes and tuberculosis syndemic in India: a narrative review of facts, gaps in care and challenges, J. Diabetes (2023), https://doi.org/10.1111/1753-0407.13427.
[8] Y. Zhang, Y. Zhu, P. Ma, H. Wu, D. Xiao, Y. Zhang, X. Sui, L. Zhang, A. Dong, Functional carbohydrate-based hydrogels for diabetic wound therapy, Carbohydr. Polym. 312 (2023) 120823, https://doi.org/10.1016/j.carbpol.2023.120823.
[9] K.-Y. Cheng, Z.-H. Lin, Y.-P. Cheng, H.-Y. Chiu, N.-L. Yeh, T.-K. Wu, J.-S. Wu, Wound healing in streptozotocin-induced diabetic rats using atmospheric-pressure argon plasma jet, Sci. Rep. 8 (2018) 12214, https://doi.org/10.1038/s41598-018-30597-1.
[10] S.S. Singh, S.K. Behera, S. Rai, S.K. Tripathy, S. Chakrabortty, A. Mishra, A critical review on nanomaterial based therapeutics for diabetic wound healing, Biotechnol. Genet. Eng. Rev. (2022), https://doi.org/10.1080/02648725.2022.2161732.
[11] S. Hasan, M.A. Hasan, M.U. Hassan, M. Amin, T. Javed, L. Fatima, Biopolymers in diabetic wound care management: a potential substitute to traditional dressings, Eur. Polym. J. 189 (2023) 111979, https://doi.org/10.1016/j.eurpolymj.2023.111979.
[12] Y. Liang, J. He, B. Guo, Functional hydrogels as wound dressing to enhance wound healing, ACS Nano 15 (2021) 12687–12722, https://doi.org/10.1021/acsnano.1c04206.
[13] L. Nie, Q. Wei, J. Li, Y. Deng, X. He, X. Gao, X. Ma, S. Liu, Y. Sun, G. Jiang, O. V. Okoro, A. Shavandi, S. Jing, Fabrication and desired properties of conductive hydrogel dressings for wound healing, RSC Adv. 13 (2023) 8502–8522, https://doi.org/10.1039/d2ra07195a.
[14] H. Wang, L.-M. Zhang, Intelligent biobased hydrogels for diabetic wound healing: a review, Chem. Eng. J. 484 (2024), https://doi.org/10.1016/j.cej.2024.149493.
[15] T. Xiang, Q. Guo, L. Jia, T. Yin, W. Huang, X. Zhang, S. Zhou, Multifunctional hydrogels for the healing of diabetic wounds, Adv. Health Mater. 13 (2024), https://doi.org/10.1002/adhm.202301885.
[16] H. Lu, N. Zhang, M. Ma, Electroconductive hydrogels for biomedical applications, WIREs Nanomed. Nanobiotechnol. 11 (2019), https://doi.org/10.1002/wnan.1568.

[17] T. Zhu, Y. Ni, G.M. Biesold, Y. Cheng, M. Ge, H. Li, J. Huang, Z. Lin, Y. Lai, Recent advances in conductive hydrogels: classifications, properties, and applications, Chem. Soc. Rev. 52 (2023) 473–509, https://doi.org/10.1039/D2CS00173J.
[18] S. Khanna, A.K. Singh, S.P. Behera, S. Gupta, Thermoresponsive BSA hydrogels with phase tunability, Mater. Sci. Eng.: C 119 (2021) 111590, https://doi.org/10.1016/j.msec.2020.111590.
[19] A. Upadhyay, R. Kandi, C.P. Rao, Injectable, self-healing, and stress sustainable hydrogel of BSA as a functional biocompatible material for controlled drug delivery in cancer cells, ACS Sustain Chem. Eng. 6 (2018) 3321–3330, https://doi.org/10.1021/acssuschemeng.7b03485.
[20] G. Navarra, C. Peres, M. Contardi, P. Picone, P.L. San Biagio, M. Di Carlo, D. Giacomazza, V. Militello, Heat- and pH-induced BSA conformational changes, hydrogel formation and application as 3D cell scaffold, Arch. Biochem. Biophys. 606 (2016) 134–142, https://doi.org/10.1016/j.abb.2016.07.020.
[21] K. Naik, P. Singh, M. Yadav, S.K. Srivastava, S. Tripathi, R. Ranjan, P. Dhar, A. K. Verma, S. Chaudhary, A.S. Parmar, 3D printable, injectable amyloid-based composite hydrogel of bovine serum albumin and Aloe vera for rapid diabetic wound healing, J. Mater. Chem. B 11 (2023) 8142–8158, https://doi.org/10.1039/D3TB01151H.
[22] G. Kougkolos, M. Golzio, L. Laudebat, Z. Valdez-Nava, E. Flahaut, Hydrogels with electrically conductive nanomaterials for biomedical applications, J. Mater. Chem. B 11 (2023) 2036–2062, https://doi.org/10.1039/D2TB02019J.
[23] H. Shinohara, A. Tiwari, Graphene: an introduction to the fundamentals and industrial applications, 2015. ⟨https://books.google.com/books?hl=en&lr=&id=v0hKCgAAQBAJ&oi=fnd&pg=PP1&dq=H.+Shinohara,+A.+Tiwari,+Graphene:+an+introduction+to+the+fundamentals+and+industrial+applications.+2015:+John+Wiley+%26+Sons.&ots=VpS_pfYvkJ&sig=D5FzzV5JuyzppXTPKq3z-ZvTH9Y⟩ (accessed May 28, 2024).
[24] J. Ma, D. Ping, X. Dong, Recent developments of graphene oxide-based membranes: a review, Membranes 7 (2017), https://doi.org/10.3390/membranes7030052.
[25] Y. Liu, J. Ding, Q. Wang, M. Wen, T. Tang, Y. Liu, R. Yuan, Y. Li, M. An, Research progress on the biomedical uses of graphene and its derivatives, N. Carbon Mater. 36 (2021) 779–791, https://doi.org/10.1016/S1872-5805(21)60073-2.
[26] J. Lin, X. Chen, P. Huang, Graphene-based nanomaterials for bioimaging, Adv. Drug Deliv. Rev. 105 (2016) 242–254, https://doi.org/10.1016/j.addr.2016.05.013.
[27] J. Yi, G. Choe, J. Park, J.Y. Lee, Graphene oxide-incorporated hydrogels for biomedical applications, Polym. J. 52 (2020) 823–837, https://doi.org/10.1038/s41428-020-0350-9.
[28] Z. Terzopoulou, G.Z. Kyzas, D.N. Bikiaris, Recent advances in nanocomposite materials of graphene derivatives with polysaccharides, Materials 8 (2015) 652–683, https://doi.org/10.3390/ma8020652.
[29] A. Razaq, F. Bibi, X. Zheng, R. Papadakis, S.H.M. Jafri, H. Li, Review on graphene-, graphene oxide-, reduced graphene oxide-based flexible composites: from fabrication to applications, Materials 15 (2022), https://doi.org/10.3390/ma15031012.
[30] S.R. Shin, C. Zihlmann, M. Akbari, P. Assawes, L. Cheung, K. Zhang, V. Manoharan, Y.S. Zhang, M. Yüksekkaya, K.T. Wan, M. Nikkhah, M.R. Dokmeci, X.S. Tang, A. Khademhosseini, Reduced graphene oxide-GelMA hybrid hydrogels as scaffolds for cardiac tissue engineering, Small 12 (2016) 3677–3689, https://doi.org/10.1002/smll.201600178.
[31] J. Park, J.H. Choi, S. Kim, I. Jang, S. Jeong, J.Y. Lee, Micropatterned conductive hydrogels as multifunctional muscle-mimicking biomaterials: graphene-incorporated hydrogels directly patterned with femtosecond laser ablation, Acta Biomater. 97 (2019) 141–153, https://doi.org/10.1016/j.actbio.2019.07.044.
[32] H. Jo, M. Sim, S. Kim, S. Yang, Y. Yoo, J.H. Park, T.H. Yoon, M.G. Kim, J.Y. Lee, Electrically conductive graphene/polyacrylamide hydrogels produced by mild chemical reduction for enhanced myoblast growth and differentiation, Acta Biomater. 48 (2017) 100–109, https://doi.org/10.1016/j.actbio.2016.10.035.
[33] W.S.Jr Hummers, R.E. Offeman, Preparation of graphitic oxide, J. Am. Chem. Soc. 80 (1958) 1339, https://doi.org/10.1021/ja01539a017.
[34] C. Gómez-Navarro, R.T. Weitz, A.M. Bittner, M. Scolari, A. Mews, M. Burghard, K. Kern, Electronic transport properties of individual chemically reduced graphene oxide sheets, Nano Lett. 7 (2007) 3499–3503, https://doi.org/10.1021/nl072090c.
[35] G. Eda, M. Chhowalla, Chemically derived graphene oxide: towards large-area thin-film electronics and optoelectronics, Adv. Mater. 22 (2010) 2392–2415, https://doi.org/10.1002/adma.200903689.
[36] B.Y.S.R. Majid, H. Ming, H. Lim, Graphene oxide and its electrochemical performance, Int. J. Electrochem Sci. 7 (2012) 4345–4351.
[37] M. Cheng, R. Yang, L. Zhang, Z. Shi, W. Yang, D. Wang, G. Xie, D. Shi, G. Zhang, Restoration of graphene from graphene oxide by defect repair, Carbon 50 (2012) 2581–2587, https://doi.org/10.1016/j.carbon.2012.02.016.
[38] S. Khanna, A.K. Singh, S.P. Behera, S. Gupta, Thermoresponsive BSA hydrogels with phase tunability, Mater. Sci. Eng.: C 119 (2021) 111590, https://doi.org/10.1016/j.msec.2020.111590.
[39] Y. Yang, J. Wang, S. Huang, M. Li, J. Chen, D. Pei, Z. Tang, B. Guo, Bacteria-responsive programmed self-activating antibacterial hydrogel to remodel regeneration microenvironment for infected wound healing, Natl. Sci. Rev. 11 (2024), https://doi.org/10.1093/nsr/nwae044.
[40] S.K. Nethi, S. Das, C.R. Patra, S. Mukherjee, Recent advances in inorganic nanomaterials for wound-healing applications, Biomater. Sci. 7 (2019) 2652–2674, https://doi.org/10.1039/C9BM00423H.
[41] N. Nguyen, Z.-H. Lin, S.R. Barman, C. Korupalli, J.-Y. Cheng, N.-X. Song, Y. Chang, F.-L. Mi, H.-L. Song, H.-W. Sung, Y.-J. Lin, Engineering an integrated electroactive dressing to accelerate wound healing and monitor noninvasively progress of healing, Nano Energy 99 (2022) 107393, https://doi.org/10.1016/j.nanoen.2022.107393.
[42] J. He, M. Shi, Y. Liang, B. Guo, Conductive adhesive self-healing nanocomposite hydrogel wound dressing for photothermal therapy of infected full-thickness skin wounds, Chem. Eng. J. 394 (2020) 124888, https://doi.org/10.1016/j.cej.2020.124888.